EUROPEAN ORGANIZATION FOR NUCLEAR RESEARCH

CERN-PPE/91-216
5 December 1991

DIRECT MEASUREMENT OF THE W-γ COUPLING AT THE CERN $\bar{p}p$ COLLIDER

The UA2 Collaboration

Bern - Cambridge - CERN - Dortmund - Heidelberg - Melbourne -
Milano - Orsay (LAL) - Pavia - Perugia - Pisa - Saclay (CEN)

J.Alitti[12], G.Ambrosini[9], R.Ansari[8], D.Autiero[11], P.Bareyre[12], I.A.Bertram[6], G.Blaylock[3,a], P.Bonamy[12], K.Borer[1], M.Bourliaud[12], D.Buskulic[8], G.Carboni[11], D.Cavalli[7], V.Cavasinni[11], P.Cenci[10], J.C.Chollet[8], C.Conta[9], G.Costa[7], F.Costantini[11], L.Cozzi[7], A.Cravero[7], M.Curatolo[11], A.Dell'Acqua[9], T.DelPrete[11], R.S.DeWolf[2], L.DiLella[3], Y.Ducros[12], G.F.Egan[6], K.F.Einsweiler[3,b], B.Esposito[11], L.Fayard[8], A.Federspiel[1], R.Ferrari[9], M.Fraternali[9], D.Froidevaux[3], G.Fumagalli[9], J.M.Gaillard[8], F.Gianotti[7], O.Gildemeister[3], C.Gössling[4], V.G.Goggi[9], S.Grünendahl[5], K.Hara[1,c], S.Hellman[3], J.Hrivnac[3], H.Hufnagel[4], E.Hugentobler[1], K.Hultqvist[3,d], E.Iacopini[11,e], J.Incandela[7], K.Jakobs[3], P.Jenni[3], E.E.Kluge[5], N.Kurz[5], S.Lami[11], P.Lariccia[10], M.Lefebvre[3], L.Linssen[3], M.Livan[9], P.Lubrano[3,10], C.Magneville[12], L.Mandelli[7], L.Mapelli[3], M.Mazzanti[7], K.Meier[3,f], B.Merkel[8], J.P.Meyer[12], M.Moniez[8], R.Moning[1], M.Morganti[11], L.Müller[1], D.J.Munday[2], M.Nessi[3], F.Nessi-Tedaldi[3], C.Onions[3], T.Pal[1], M.A.Parker[2], G.Parrour[8], F.Pastore[9], E.Pennacchio[9], J.M.Pentney[3], M.Pepe[3], L.Perini[7], C.Petridou[11], P.Petroff[8], H.Plothow-Besch[3], G.Polesello[3,9], A.Poppleton[3], K.Pretzl[1], M.Primavera[11,g], M.Punturo[10], J.P.Repellin[8], A.Rimoldi[9], M.Sacchi[9], P.Scampoli[10], J.Schacher[1], B.Schmidt[4], V.Simak[3], S.L.Singh[2], V.Sondermann[4], R.Spiwoks[4], S.Stapnes[3], C.Talamonti[10], F.Tondini[10], S.N.Tovey[6], E.Tsesmelis[4], G.Unal[8], M.Valdata-Nappi[11,g], V.Vercesi[9], A.R.Weidberg[3,h], P.S.Wells[2,i], T.O.White[2], D.R.Wood[8], S.A.Wotton[2,i], H.Zaccone[12], A.Zylberstejn[12]

(Submitted to Physics Letters B)

Abstract

The process $\bar{p}p \rightarrow e\nu\gamma + X$ is studied at $\sqrt{s} = 630$ GeV. The observed signal is used to extract a direct measurement of the parameters κ and λ which define the magnetic dipole and electric quadrupole moments of the W boson and therefore the $WW\gamma$ coupling. We find $\kappa = 1^{+2.6}_{-2.2}$ and $\lambda = 0^{+1.7}_{-1.8}$ and their 95% confidence limits $-3.5 < \kappa < 5.9$ and $-3.6 < \lambda < 3.5$. The results are model independent and in good agreement with the Standard Model values, $\kappa = 1$ and $\lambda = 0$.

1 Laboratorium für Hochenergiephysik, Universität Bern, Sidlerstraße 5, 3012 Bern, Switzerland
2 Cavendish Laboratory, University of Cambridge, Cambridge, CB3 0HE, UK
3 CERN, 1211 Geneva 23, Switzerland
4 Lehrstuhl für Exp. Physik IV, Universität Dortmund, 4600 Dortmund, FRG
5 Institut für Hochenergiephysik der Universität Heidelberg, Schröderstraße 90, 6900 Heidelberg, FRG
6 School of Physics, University of Melbourne, Parkville 3052, Australia.
7 Dipartimento di Fisica dell'Università di Milano and Sezione INFN Milano, 20133 Milano, Italy
8 Laboratoire de l'Accélérateur Linéaire, Université de Paris-Sud, 91405 Orsay, France
9 Dipartimento di Fisica Nucleare e Teorica, Università di Pavia and INFN, Sezione di Pavia, Via Bassi 6, 27100 Pavia, Italy
10 Dipartimento di Fisica dell'Università di Perugia and INFN, Sezione di Perugia, via Pascoli, 06100 Perugia, Italy
11 Dipartimento di Fisica dell'Università di Pisa and INFN, Sezione di Pisa, Via Livornese, S.Piero a Grado, 56100 Pisa, Italy
12 Centre d'Etudes Nucléaires de Saclay, 91191 Gif-sur-Yvette Cedex, France

a) Now at University of California, Santa Cruz, California, USA
b) Now at Lawrence Berkeley Laboratory, Berkeley, California, USA
c) Now at University of Tsukuba, Tsukuba, Ibaraki 305, Japan
d) Now at University of Stockholm, Stockholm, Sweden
e) Also at Scuola Normale Superiore, Pisa, Italy
f) Now at Deutsches Elektronen Synchrotron, Hamburg, FRG
g) Now at Dipartimento di Fisica dell'Università della Calabria e gruppo INFN, Cosenza, Italy
h) Now at Nuclear Physics Laboratory, University of Oxford, Oxford, UK
i) Now at CERN, Geneva, Switzerland.

1. INTRODUCTION

The gauge boson couplings to fermions are at present being tested with ever increasing accuracy. However the self interactions among gauge bosons (WWγ, WWZ vertices) are still awaiting direct experimental tests. The experimental study of the self-coupling of the electroweak bosons will enable us to understand whether their self-interactions are constrained by the SU(2) × U(1) gauge symmetry. This would not be the case if they were composite particles.

In the Standard Model the WWγ vertex is uniquely determined by requiring $SU(2)_L \times U(1)_Y$ gauge invariance. The most general WWγ vertex that one can consider has to fulfil U(1) and Lorentz gauge invariance. These two constraints allow for four free independent parameters in the theory. If we also assume CP invariance there are two parameters left (κ, λ), which are related to the magnetic dipole (μ_W) and electric quadrupole (Q_W) moments of the W boson by the equations:

$$\mu_W = \frac{e}{2M_W}(1+\kappa+\lambda) \tag{1}$$

$$Q_W = -\frac{e}{M_W^2}(\kappa-\lambda) \tag{2}$$

In the Standard Model, the values for κ and λ are fixed : $\kappa = 1, \lambda = 0$. Even before the discovery of the W and Z bosons, it was suggested [1] that the magnetic moment of the W is an interesting property to measure, and that the reaction $\bar{p}p \rightarrow W\gamma + X$ is a good candidate for this measurement especially because it was found [2] that the angular distribution of the W bosons is particularly sensitive to μ_W and consequently to the parameters κ and λ. Many predictions have since been made for hadron and ep collisions [3-5] as well as for e^+e^- machines [6,7] of the possibility of measuring the WWZ and WWγ couplings at existing and future colliders.

Motivated by the present theoretical interest we study the process $\bar{p}p \rightarrow e\nu\gamma + X$ at the CERN $\bar{p}p$ collider and report here a first measurement of the κ and λ parameters. The lowest order diagrams contributing to this process are shown in Fig.1. Diagram a) corresponds to what we will refer to from now on as the W-radiative decay while diagrams b), c) and d) describe W-γ production. The cross section of the process depends upon the parameters κ and λ through diagram c) and its interference with other diagrams. Some consequences of possible anomalous moments of the W boson are :

- If κ or λ take values different from those predicted by the Standard Model, the cross section for the process $q\bar{q}' \rightarrow e\nu\gamma$ increases. Thus any excess of events measured in this channel will be an indication for physics outside the Standard Model.
- The differential distributions of some kinematical variables depend strongly on κ, λ. Such variables are, for example, the transverse momentum of the photon (p_T^γ), the invariant mass of the Wγ system ($M_{W\gamma}$), the transverse mass of the e$\gamma\nu$ system ($m_T^{e\gamma\nu}$) and the angular distribution of the W boson in the quark-antiquark centre of mass system ($\cos\theta_W^*$). At the energy of the CERN $\bar{p}p$ collider, due to limited statistics, one cannot measure these distributions accurately. However, in the immediate future (HERA and TeVatron) as well as at future colliders (LEP200, LHC and SSC), they could provide clear evidence for deviations from the Standard Model [4,8].

In this article we report on a search for events containing an electron, a neutrino and a photon in the entire data sample collected during the period 1988-90, corresponding to an integrated luminosity of 13 pb^{-1}. After subtracting the background, we compare the observed signal with Monte Carlo predictions for various values of κ and λ and obtain their values by a best-fit procedure.

2. THE UA2 DETECTOR

A detailed description of the upgraded UA2 detector can be found in Ref. [9]. In this Letter we present a brief outline of the apparatus with emphasis on the detector components relevant to this analysis.

The calorimeters cover the pseudorapidity range $-3 \leq \eta \leq 3$. The central calorimeter [10] extends up to η of ± 1 while the rest is covered by the end cap calorimeters. Both calorimeters are made of lead and iron absorber plates, sandwiched with scintillator plates, and are read out by wavelength shifters. The central calorimeter is longitudinally segmented into an electromagnetic compartment (17 radiation lengths) with lead absorber and two hadronic compartments (with a depth of two interaction lengths each) with iron absorber. The end caps consist of an electromagnetic compartment (17-24.4 radiation lengths deep, depending on the polar angle) and a hadronic compartment (6.2-7 interaction lengths deep).

The lateral segmentation in the central calorimeter is constant in azimuth ($\Delta\phi = 15°$) and polar ($\Delta\theta = 10°$) angles. In the end caps, the two cells closest to the

beam axis ($2.5 < |\eta| < 3.0$ and $2.2 < |\eta| < 2.5$) cover 30° in azimuth, and the other cells have a constant segmentation $\Delta\phi = 15°$, $\Delta\eta = 0.2$. The electromagnetic compartments of the outermost cells of the central calorimeter (edge cells), which cover $0.8 < |\eta| < 1.0$, are shortened to accommodate the inner detectors and consequently have a degraded performance.

Energy clusters in the calorimeter are reconstructed by joining all cells which share a common edge and contain an energy greater than 400 MeV. A cluster is considered electromagnetic if its lateral size and the energy leakage into the hadronic compartments are small. These clusters are then examined as potential electron or photon candidates.

The central detector, located inside the central calorimeter, consists of a series of concentric cylindrical subdetectors. Around the beam pipe, at radii of 3.5 cm (inner) and 14.5 cm (outer), are two arrays of silicon counters used for tracking and ionization measurements [11]. Between them is a cylindrical drift chamber of jet geometry [12] and after the outer silicon layer is the Transition Radiation Detector [13]. The outermost of the central detectors is the Scintillating Fibre Detector (SFD) [14]. It contains approximately 60 000 fibres arranged on cylinders into 8 stereo triplets. The last two triplets of the SFD are located after 1.5 radiation lengths of lead and are used as 'preshower detector', to localize the early development of electromagnetic showers. In the end cap region tracking and preshower detection is accomplished by the end cap proportional tubes [15]. For the present analysis only events with electromagnetic clusters in the central region ($-1 \leq \eta \leq 1$) are considered.

The $\bar{p}p$ collisions take place in the centre of the detector with an *rms* spread along the beam direction of 130 mm. A minimum bias trigger is obtained from the Time-of-Flight counters, while the luminosity is measured using eight scintillator telescopes at small angles to the beams.

3. EVENT SELECTION

The data were taken in a series of runs during the 1988 to 1990 CERN $\bar{p}p$ collider operation at an energy $\sqrt{s} = 630$ GeV, and represent the entire sample collected with the upgraded UA2 detector, which corresponds to an integrated luminosity of 13.0 $\pm$ 0.7 pb^{-1}. The signature for $\bar{p}p \rightarrow e\nu\gamma + X$ is an electron, missing transverse momentum ($\not{p}_T$) and a photon.

3.1. Electron Identification

The electron identification and electron selection efficiencies have been extensively described in Refs. [9,16]. Here we briefly describe the procedure and we give at each step the estimated efficiency, as measured for the entire running period. The existence of an electromagnetic cluster (small lateral size and leakage into the hadronic compartment) in the central calorimeter is required. The cuts on the lateral and longitudinal profile of the cluster are applied at the trigger level (91.7 ± 1.0%). The electron candidate must also have a track reconstructed in the central detectors, associated with the electromagnetic cluster. The track must originate from a vertex reconstructed within 250 mm from the centre of the detector along the beam direction. In addition, a reconstructed preshower cluster must match the track of the electron candidate (77.2 ± 1.7%). Once the precise track trajectory is found, a χ^2 test is performed on the electromagnetic cluster (93.5 ± 1.0%), requiring that the lateral and longitudinal profile of the shower in the calorimeter be consistent with an electron incident along the track direction as measured in a test beam. The efficiencies as given above were measured using electrons from a test beam and from W decays [16]. The overall efficiency to detect an isolated electron in the data was measured to be 66.2 ± 2.2%.

3.2. Neutrino Identification

The neutrino transverse energy in the event is obtained by measuring the electron energy and the energies of all other particles (mainly hadrons) in the event. The missing transverse momentum ($\not{p}_T$) is then attributed to the undetected neutrino :

$$\vec{p}^{\,\nu}_T \equiv \vec{\not{p}}_T = - \vec{p}^{\,e}_T - \vec{p}^{\,had}_T . \qquad (3)$$

$\vec{p}^{\,e}_T$ is the reconstructed electron transverse momentum and $\vec{p}^{\,had}_T$ is the total transverse momentum of all other particles as computed by the equation:

$$\vec{p}^{\,had}_T = (\Sigma E_{cell}\ \hat{v}_{cell})_T \qquad (4)$$

where E_{cell} is the energy in a given calorimeter cell and $\hat{v}_{cell}$ is a unit vector from the interaction vertex to the centre of the cell. The sum extends over all calorimeter cells excluding those assigned to the electron.

3.3. Photon Identification

For the photon candidate we require the existence of an electromagnetic cluster (besides the cluster of the electron candidate), separated in space from the electron by at least 15° and with a $p_T > 4.5$ GeV. This second electromagnetic cluster must also be in the central pseudorapidity region ($-1 \leq \eta \leq 1$). Furthermore, we require that there be no track reconstructed in a 10° cone around the direction defined by the event vertex and the centroid of the electromagnetic cluster. In order to estimate the photon detection efficiency in the presence of a nearby electron as a function of the photon energy and its impact point on a calorimeter cell, we overlay test beam electrons of different energies and impact points on a calorimeter cell onto $W \rightarrow e\nu$ candidate events and reanalyse them. An analytic form for the efficiency is derived as a function of the space angle between electron and photon, and is then used with the Monte Carlo generated events for the process $q\bar{q}' \rightarrow e\nu\gamma$.

In estimating the photon efficiency, we must also take into account the probability of losing a photon candidate because of random tracks inside the 10° cone around the photon direction. This probability was computed using $W \rightarrow e\nu$ events and counting how often we find at least one track in a 10° cone randomly oriented away from the electron direction. This effect reduced the relative photon detection efficiency to $89.7 \pm 1.1\%$.

3.4. Selection Criteria

The following kinematical requirements were imposed to select $e\nu\gamma$ candidates : $p_T^e > 20$ GeV, $p_T^\gamma > 4.5$ GeV, $p_T^\nu > 20$ GeV and the transverse mass of the $e\nu$ system $m_T > 40$ GeV, where $m_T^2 \equiv 2\, p_T^e\, p_T^\nu\, (1 - \cos\phi^{e\nu})$ and $\phi^{e\nu}$ is the azimuthal separation between the electron and neutrino directions. The selection for p_T^e, p_T^ν and m_T is identical to that for W candidate events as presented in Ref. [16]. The additional requirement for a photon candidate in the event reduces the initial sample of 2887 W events to 16, which are the candidates for the process $q\bar{q}' \rightarrow e\nu\gamma$. The transverse energy flow of one of these candidates is shown in Fig. 2.

4. BACKGROUND ESTIMATE

The main source of background is $W \rightarrow e\nu$ decays associated with jets, where a jet is misidentified as a photon. In order to estimate this background we need to know the probability that a jet in the UA2 detector is taken to be a photon. This probability is computed as a function of the jet p_T as follows. From a sample of hadronic events selected by requiring the presence of an electromagnetic cluster in the central calorimeter, we compute the fraction of the events having a second electromagnetic cluster with $|\eta| \leq 1$ and a given p_T ($p_T \geq 4.5$ GeV), which fulfils the photon selection criteria. This probability is shown in Fig. 3a as a function of the p_T of the second electromagnetic cluster. It can be parametrized by a function of the form

$$f(p_T) = A \cdot e^{-\beta p_T} \tag{5}$$

where $A = 0.039 \pm 0.0013$ and $\beta = 0.153 \pm 0.004$ GeV^{-1}. We then apply this probability to the p_T distribution of all jets associated with $W \rightarrow e\nu$ events collected in the 1988-90 running period (2887 events). The p_T distribution of all jets associated with the $W \rightarrow e\nu$ events is shown in Fig. 3b (histogram), together with the distribution folded with the probability function (5) (solid curve). The latter represents the p_T shape of the background. Its integral is 6.8 ± 1 events and corresponds to the total number of background events expected in the final sample of 16 events. The error combines linearly a statistical uncertainty from the number of jets and a systematic error from the fit.

5. RESULTS AND DISCUSSION

Given 16 observed events in the entire (1988-90) sample, and the number of background events (6.8 ± 1) as computed in the previous section (using a simple calculation based on Poisson statistics [17] which takes into account the error on the background), we compute a signal of

$$N_S = 9.2^{+5.2}_{-3.2}\,. \tag{6}$$

The 95% confidence interval for the signal is

$$2.9 < N_S < 19.3. \tag{7}$$

The experimental results are then compared with Monte Carlo predictions for the Standard Model values of $\kappa = 1$ and $\lambda = 0$. Two different Monte Carlo calculations were used [4,18] whose agreement for any values of κ and λ is better than 1%. In both simulations the process $q\bar{q}' \rightarrow e\nu\gamma$ is generated only to lowest order and therefore the cross section for the process has the uncertainty due to higher order corrections. To minimize this uncertainty we proceed as follows. The standard UA2 Monte Carlo for the process $W \rightarrow e\nu$ contains also the radiation of a photon by the electron, as given in Ref. [19]. By normalizing the Monte Carlo result to the inclusive cross section for $W \rightarrow e\nu$ production [16], we obtain the W-radiative decay cross section. From this procedure we estimate a systematic uncertainty of 5% to the Monte Carlo prediction.

The Monte Carlo events first undergo the UA2 detector simulation, which accounts for energy resolution in the calorimeter and the electron-photon angular separation efficiency. A further correction of $51.9 \pm 1.9\%$ is made for the global event efficiency which contains all factors not included in the simulation. This number is dominated by the electron efficiency ($66.2 \pm 2.2\%$) and by the photon selection efficiency given in Section 3.3 ($89.7 \pm 1.1\%$). The rest accounts for vertex and trigger inefficiencies as described in Ref. [16].

After these corrections, for a total luminosity of 13.0 ± 0.7 pb^{-1}, the Monte Carlo predicts 11.9 ± 1.1 events for the Standard Model, in good agreement with the number of events as computed from the data (eq. 6). The error represents the systematic uncertainty discussed below. In Fig. 4 we compare the distributions of some of the relevant kinematical variables as found in the data (16 events) with those obtained by adding the background shape to the Monte Carlo prediction. Given the limited statistics the agreement is good. The cumulative Kolmogorov statistics test, performed on the distributions, gives a probability of greater than 70% on all the variables.

To extract limits for the κ, λ variables, we compare the Monte Carlo prediction for various κ, λ values with the observed signal. The expected number of events has a minimum at the Standard Model values of κ and λ and increases for κ, λ away from these values. The results are consistent with this minimum number of events as given by the Standard Model. In Fig. 5a, the Monte Carlo predicted number of events is given as a function of κ keeping λ at its Standard Model value. Similarly, in Fig. 5b the observed signal is compared to the Monte Carlo prediction for different λ keeping $\kappa = 1$. We obtain

$$\kappa = 1^{+4.6}_{-4.2} \pm 1.0(\text{syst}) \qquad \text{and} \qquad \lambda = 0^{+2.9}_{-2.9} \pm 0.7(\text{syst}). \tag{8}$$

The 95% confidence level limits on κ, λ are :

$$-5.3 < \kappa < 7.9 \quad \text{for} \quad \lambda = 0 \quad \text{and} \quad -4.4 < \lambda < 4.4 \quad \text{for} \quad \kappa = 1. \qquad (9)$$

The systematic uncertainty in the theoretical predictions is indicated in Figs. 5a and 5b as the band defined by the two extreme parabolae and amounts to 9%. This was obtained by adding in quadrature a systematic uncertainty on the Monte Carlo prediction of 7% which includes a 4.5% uncertainty due to the structure functions [20], a 4% error on the efficiency of the electron-photon angular separation, and a 4% uncertainty on the cut on p_T^{γ} at 4.5 GeV. The central values of the Monte Carlo predictions were obtained with the parton density parametrizations of HMRSB [21].

A significant improvement to the above limits can be obtained using a maximum likelihood method to compare the p_T^{γ} distribution between data and Monte Carlo predictions with the background expectation added to it, see Fig. 4a. The method exploits the fact that hard photons are a signature for possible anomalous moments of the W-boson [4], while no such photons are observed in the data sample. The likelihood from the bin-by-bin comparison of the p_T^{γ} spectrum between data and expectation is computed for various values of κ and λ keeping the other variable fixed at its Standard Model value. Their distributions are nearly Gaussian. The values found by this method are

$$\kappa = 1^{+2.6}_{-2.2} \qquad \text{and} \qquad \lambda = 0^{+1.7}_{-1.8} . \qquad (10)$$

The 95% confidence limits are

$$-3.5 < \kappa < 5.9 \quad \text{for} \quad \lambda = 0 \quad \text{and} \quad -3.6 < \lambda < 3.5 \quad \text{for} \quad \kappa = 1. \qquad (11)$$

The 68% and 95% confidence limit contours in the κ,λ plane as computed by the likelihood method are shown in Fig. 5c.

Previous indirect limits on the magnetic dipole and electric quadrupole moments of the W boson have been obtained from :

- The measurement of the anomalous magnetic moment of the muon [22-25]. The contribution of κ and λ to the anomalous magnetic moment of the muon cannot exceed the difference between the current experimental measurement of the muon g - 2 and the value predicted by the Standard Model. However, the non Standard

Model contribution to g - 2 contains divergent loop diagrams. As a consequence, the limits on κ and λ depend on the cutoff and regularization scheme used in the calculation.

- The possible compositeness of the photon propagator or of the W boson. The photon structure, for example, is affected by contributions due to the magnetic moment of the W. The limits in this case depend on the compositeness scale assumed [26].

- The mass ratio of the W and Z bosons. These limits are expressed as deviations of the ρ-parameter ($\rho = \frac{M_W^2}{M_Z^2 \cdot \cos^2\theta_W}$) from its Standard Model value of unity [23],

  but are controversial [26,27], because the ρ parameter is also sensitive to other deviations from the Minimal Standard Model.

- Unitarity constraints. Tree level partial wave unitarity, applied to fermion pair annihilation into Wγ (or WZ, or WW), constrains the κ, λ parameters [28,23]. These limits are also cutoff-dependent as discussed below.

The only direct experimental limits on κ, λ are from previous searches at PEP and PETRA, where the process $e^+e^- \rightarrow \nu\bar{\nu}\gamma$ has been studied, providing very weak limits on κ ($-75 \leq \kappa \leq 37$) [29].

The question arises whether this present measurement is model independent. Any theory using values of κ and λ different from the Standard Model values is non-renormalizable and therefore the calculation must be constrained to fulfil unitarity at tree level [28]. To ensure that the cross section due to the anomalous couplings does not grow beyond the unitarity bound, a cutoff scale is introduced which forces κ and λ to resume their Standard Model values at asymptotically large energies. A deviation from $\kappa = 1$, $\lambda = 0$ can be described by a form factor which vanishes at large Wγ invariant masses. This implies that the cross section for various κ, λ depends on the cutoff scale Λ used in the theory which in turn indicates the energy scale at which the W boson has a composite structure. Figure 6 shows the differential cross section ($d\sigma / dM_{W\gamma}$) times the branching ratio, for $W \rightarrow e\nu$ as a function of the Wγ invariant mass at $\sqrt{s} = 630$ GeV, for the Standard Model, for $\kappa = 8$ and no cutoff ($\Lambda = \infty$) and for $\kappa = 8$ and $\Lambda = 1$ TeV. On the same figure the unitarity bound is also shown. It can be

seen that even for $\kappa = 8$ the unitarity limit is not reached at $\sqrt{s} = 630$ GeV and the cross section of the process is independent of Λ. This, however, is not the case for the large $\sqrt{s}$ values at the future hadron colliders (LHC and SSC), where already at small deviations of κ and λ from the Standard Model values the unitarity limit is reached and a cutoff is needed [4].

It is therefore important to stress that these new values of κ and λ are model independent and below the unitarity limit.

6. CONCLUSIONS

A first direct measurement of the coupling of the W boson to the photon has been performed at the CERN $\bar{p}p$ collider. The parameter κ has been measured to be $1^{+2.6}_{-2.2}$ with $-3.5 < \kappa < 5.9$ as its 95% confidence limits. The parameter λ has been measured to be $0^{+1.7}_{-1.8}$ with $-3.6 < \lambda < 3.5$ as its 95% confidence limits. The measurements do not depend on any cutoffs or regularization schemes and are in good agreement with expectations from the Standard Model.

ACKNOWLEDGEMENTS

We thank our theory colleagues R. Barbieri, U. Baur and C. Papadopoulos for fruitful discussions and the latter two for also providing us with their detailed calculations as well as the code of their Monte Carlo simulations.

The technical staff of the institutes collaborating in UA2 have contributed substantially to the construction and operation of the experiment. We deeply thank them for their support. The experiment would not have been possible without the very successful operation of the improved CERN $\bar{p}p$ Collider, whose staff and coordinators we sincerely thank for their collective effort.

Financial support from the Schweizerischen Nationalfonds zur Förderung der Wissenschaftlichen Forschung to the Bern group, from the UK Science and Engineering Research Council to the Cambridge group, from the Bundesministerium für Forschung und Technologie to the Dortmund and Heidelberg groups, from the Australian Research Council, the CRA Pty Ltd, and the Victorian Education Foundation to the Melbourne group, from the Institut National de Physique Nucléaire et de Physique des Particules to the Orsay group, from the Istituto Nazionale di Fisica Nucleare to the Milano, Pavia, Perugia and Pisa groups and from the Institut de Recherche Fondamentale (CEA) to the Saclay group are acknowledged.

REFERENCES

[1] K.O. Mikaelian, Phys. Rev. D17 (1978) 750.

[2] K.O. Mikaelian, M.A. Samuel and D. Sahdev, Phys. Rev. Lett. 43 (1979) 746.

[3] J. Cortes, K. Hagiwara and F. Herzog, Nucl. Phys. B278 (1986) 26.

[4] U. Baur and D. Zeppenfeld, Nucl. Phys. B308 (1988) 127.

[5] U. Baur and D. Zeppenfeld, Nucl. Phys. B325 (1989) 253;
U. Baur et al., Proceedings of The Large Hadron Collider Workshop, CERN 90-10, ECFA 90-133, Vol II, (1990) 956.
U. Baur, J.A.M. Vermaseren, and D. Zeppenfeld, FSU-HEP-911028, MAD/PH/675, October 1991.

[6] K. Hagiwara, R.D. Peccei, D. Zeppenfeld and K. Hikasa, Nucl. Phys. B282 (1987) 253.

[7] D. Zeppenfeld, Phys. Lett. B183 (1987) 380.

[8] H. Kuijf et al., Proceedings of The Large Hadron Collider Workshop, CERN 90-10, ECFA 90-133, Vol II, (1990) 91.

[9] J. Alitti et al., Z. Phys. C47 (1990) 11.

[10] A. Beer et al., Nucl. Instr. and Meth. A224 (1984) 360.

[11] R. Ansari et al., Nucl. Instr. Meth. A279 (1989) 388.

[12] F. Bosi et al., Nucl. Instr. Meth. A283 (1989) 532.

[13] R. Ansari et al., Nucl. Instr. Meth. A263 (1988) 51.

[14] R.E. Ansorge et al., Nucl. Instr. Meth. A265 (1988) 33;
J. Alitti et al., Nucl. Instr. Meth. A279 (1989) 364.

[15] K. Borer et al., Nucl. Instr. Meth. A286 (1990) 128.

[16] J. Alitti et al., CERN-PPE/91-162, Submitted to Phys. Lett.

[17] Particle Data Group: Review of Particle Properties, Phys. Lett. B204 (1988) 81;
G. Zech, Nucl. Instr. Meth. A277 (1989) 608.

[18] E.N. Argyres, O. Korakianitis, C.G. Papadopoulos and W.J. Stirling, Phys. Lett. B259 (1991) 195.

[19] F.A. Berends and R. Kleiss, Z. Phys C27 (1985) 365.

[20] H. Plothow-Besch, Parton Density Functions, Proceedings of the 3rd Workshop on Detector and Event Simulation in High Energy Physics (Amsterdam, April 1991).

[21] P.N. Harriman, A.D. Martin, R.G. Roberts and W.J. Stirling, Phys. Rev. D42 (1990) 798.

[22] F. Herzog, Phys. Lett. 148B (1984) 355;
Erratum F. Herzog, Phys. Lett. 155B (1984) 468.

[23] M. Suzuki, Phys. Lett. 153B (1985) 289.

[24] A. Grau and J.A. Grifols, Phys. Lett. 148B (1984) 358;
A. Grau and J.A. Grifols, Phys. Lett. 154B (1985) 283.
[25] J.C. Wallet, Phys. Rev. D 32 (1985) 813.
[26] J.J. van der Bij, Phys. Rev. D35 (1987) 1088.
[27] J.A. Grifols, S. Peris and J. Sola, Int. Journ. Mod. Phys. A3 (1988) 225.
[28] U. Baur and D. Zeppenfeld, Phys. Lett. B201 (1988) 383.
[29] H. Grotch and R.W. Robinett, Phys. Rev. D36 (1987) 2153.

FIGURE CAPTIONS

Fig. 1 Lowest order Feynman diagrams for the process $q\bar{q}' \rightarrow e\nu\gamma$.

Fig. 2 Transverse energy flow distribution ("Lego" plot) of a $W + \gamma$ candidate.

Fig. 3 a) The probability for a QCD jet to be identified as a photon in the UA2 detector, as a function of the p_T of the jet cluster. The fit to the distribution is superimposed.
b) The p_T distribution of all clusters associated to the W candidate events (histogram). The background distribution, contributing to the $W \rightarrow e\nu\gamma$ process, see text, is also shown (solid curve).

Fig. 4 a) The photon transverse momentum distribution (P_T^{γ}), b) the space angle between electron and photon ($\Delta A^{e\gamma}$) and c) the transverse mass of the of the electron-photon-neutrino system ($M_T^{e\gamma\nu}$) for the 16 candidate events (histogram). Superimposed on a), b), and c) (solid curves) are the Standard Model prediction added to the estimated background shapes.

Fig. 5 The Monte Carlo predictions for the number of expected events in the UA2 detector for a), various κ values when $\lambda = 0$, and b) for λ values when $\kappa = 1$. The UA2 data point and its error are also given. The bands define the 9% estimated uncertainty to the theoretical predictions. c) The 68% and 95% confidence limit contours in the κ, λ plane from the maximum likelihood method.

Fig. 6 The differential cross section with respect to the $W\gamma$ invariant mass times the branching ratio for $W \rightarrow e\nu$ at $\sqrt{s} = 630$ GeV. The dotted curve is the Standard Model prediction. The continuous line is the unitarity bound. The dashed and dash-dotted curves are the Monte Carlo predictions for $\kappa = 8$ and cutoff (Λ) set to ∞ and 8 TeV respectively.

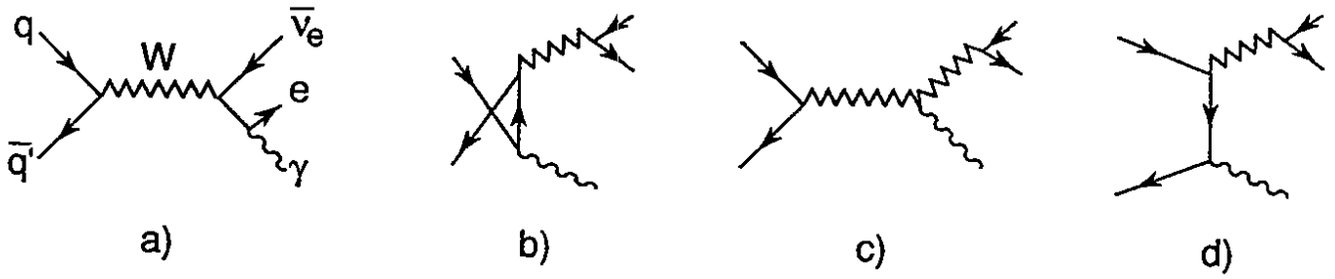

FIG. 1

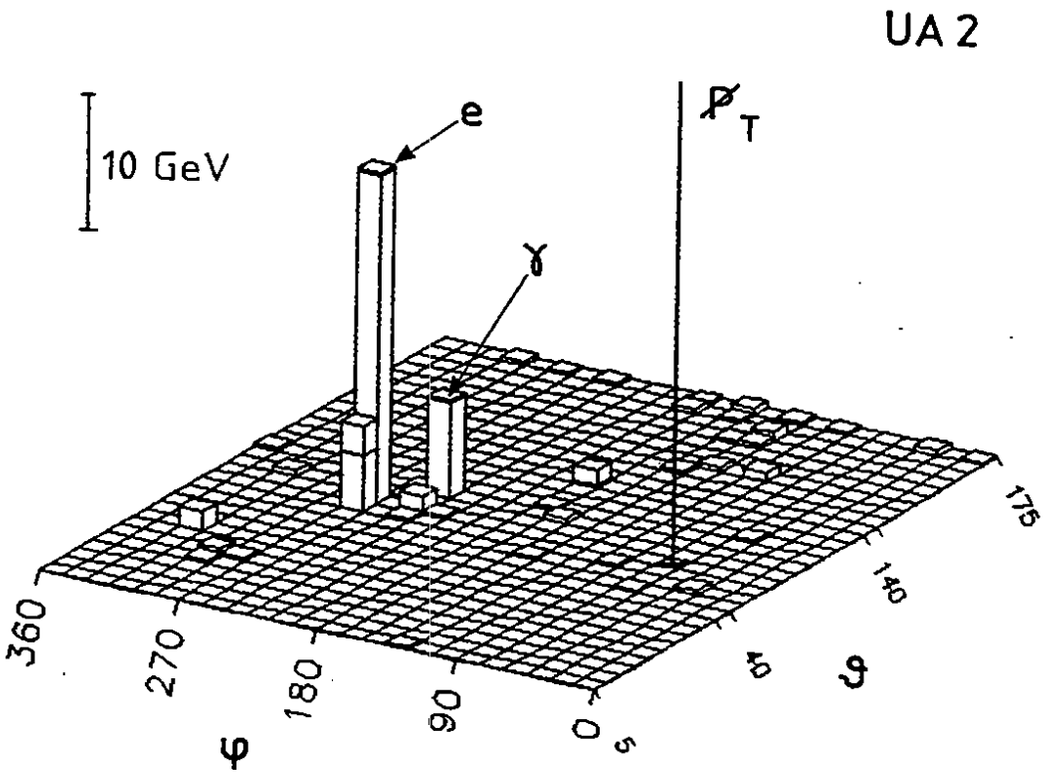

FIG. 2

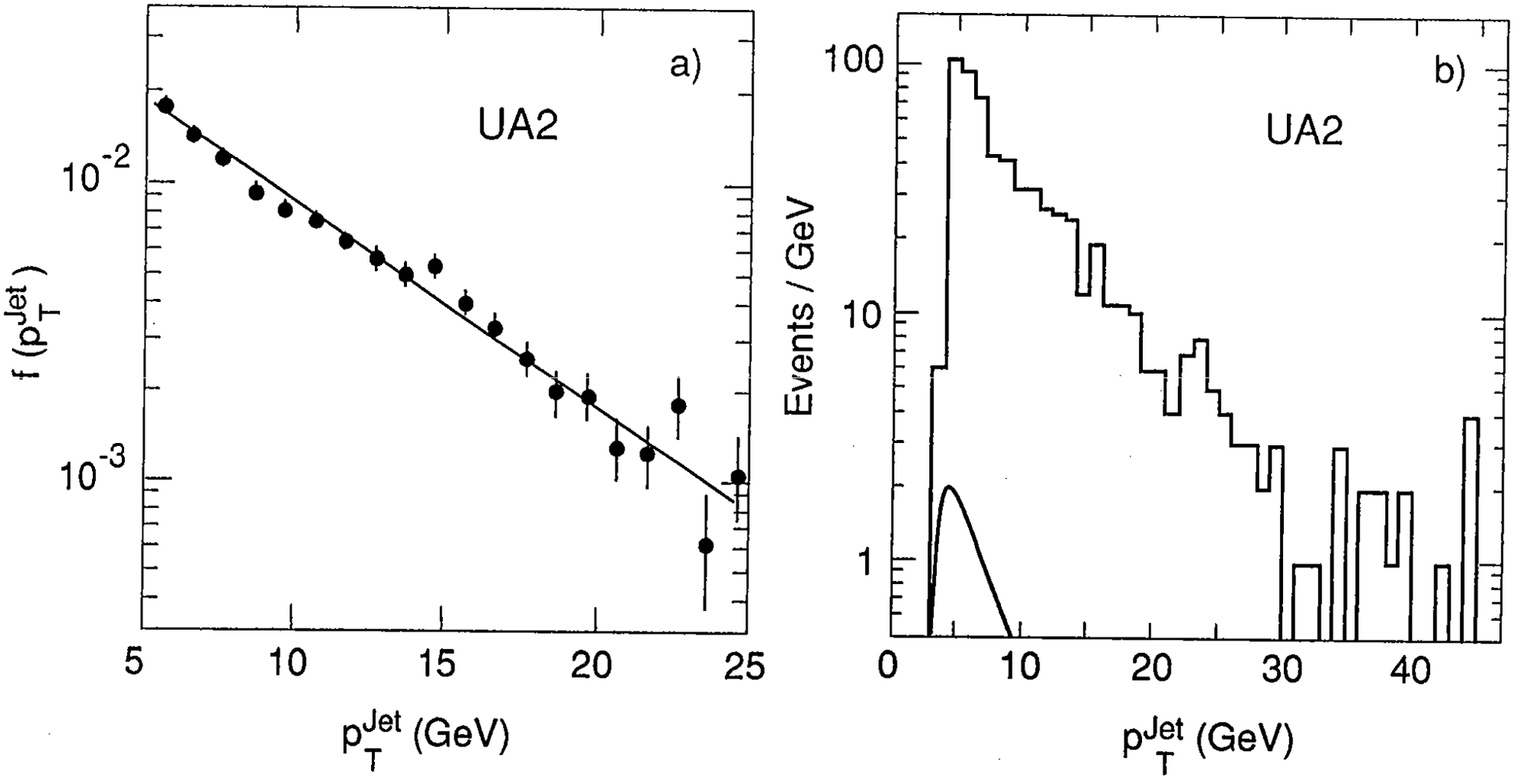
a)
UA2
10^{-2}
10^{-3}
$f(p_T^{Jet})$
5
10
15
20
25
p_T^{Jet} (GeV)
b)
UA2
100
10
1
Events / GeV
0
10
20
30
40
p_T^{Jet} (GeV)

FIG. 3

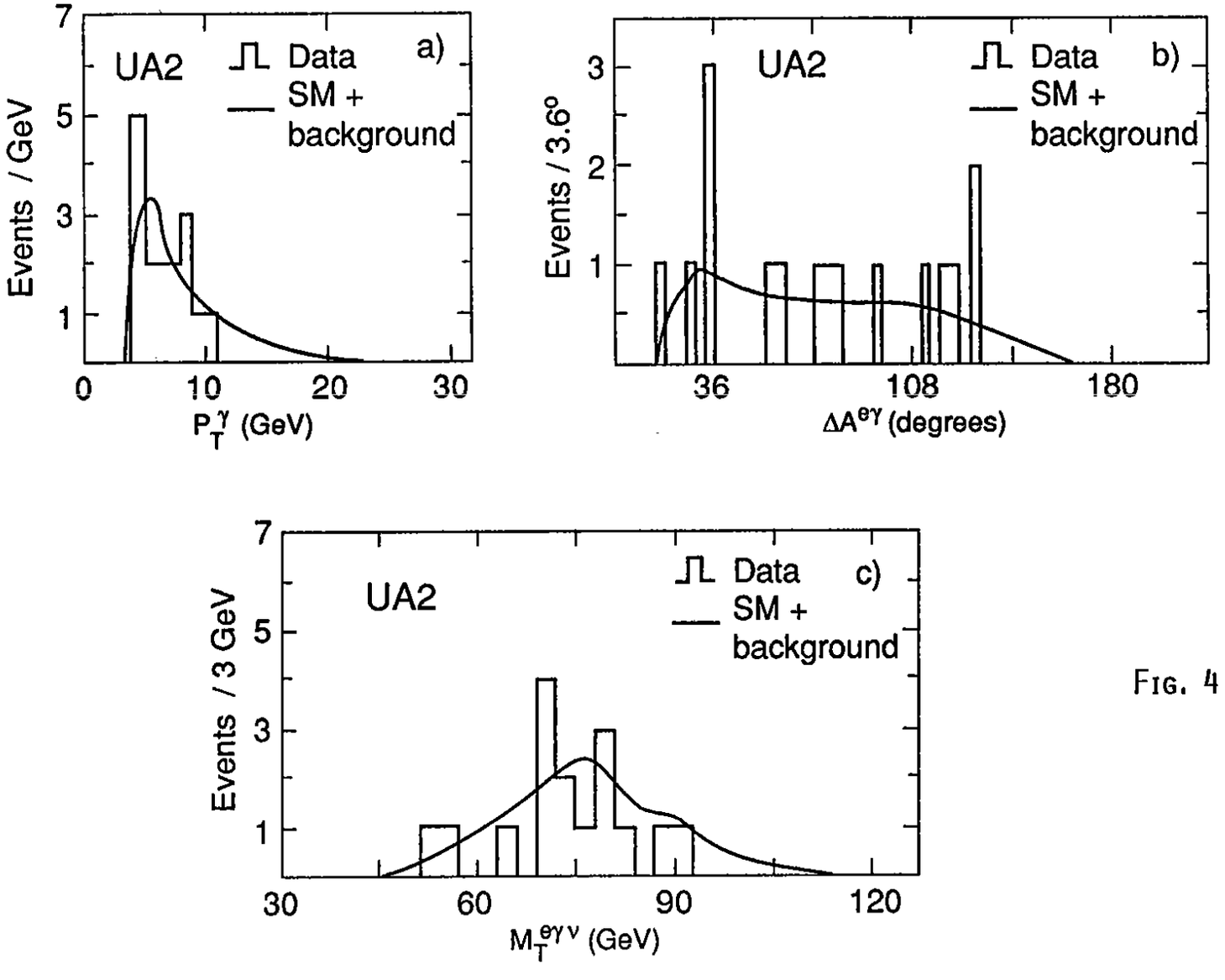
UA2
Data
SM + background
a)
Events / GeV
P_T^γ (GeV)
b)
Events / 3.6°
$\Delta A^{e\gamma}$ (degrees)
c)
Events / 3 GeV
$M_T^{e\gamma\nu}$ (GeV)

FIG. 4

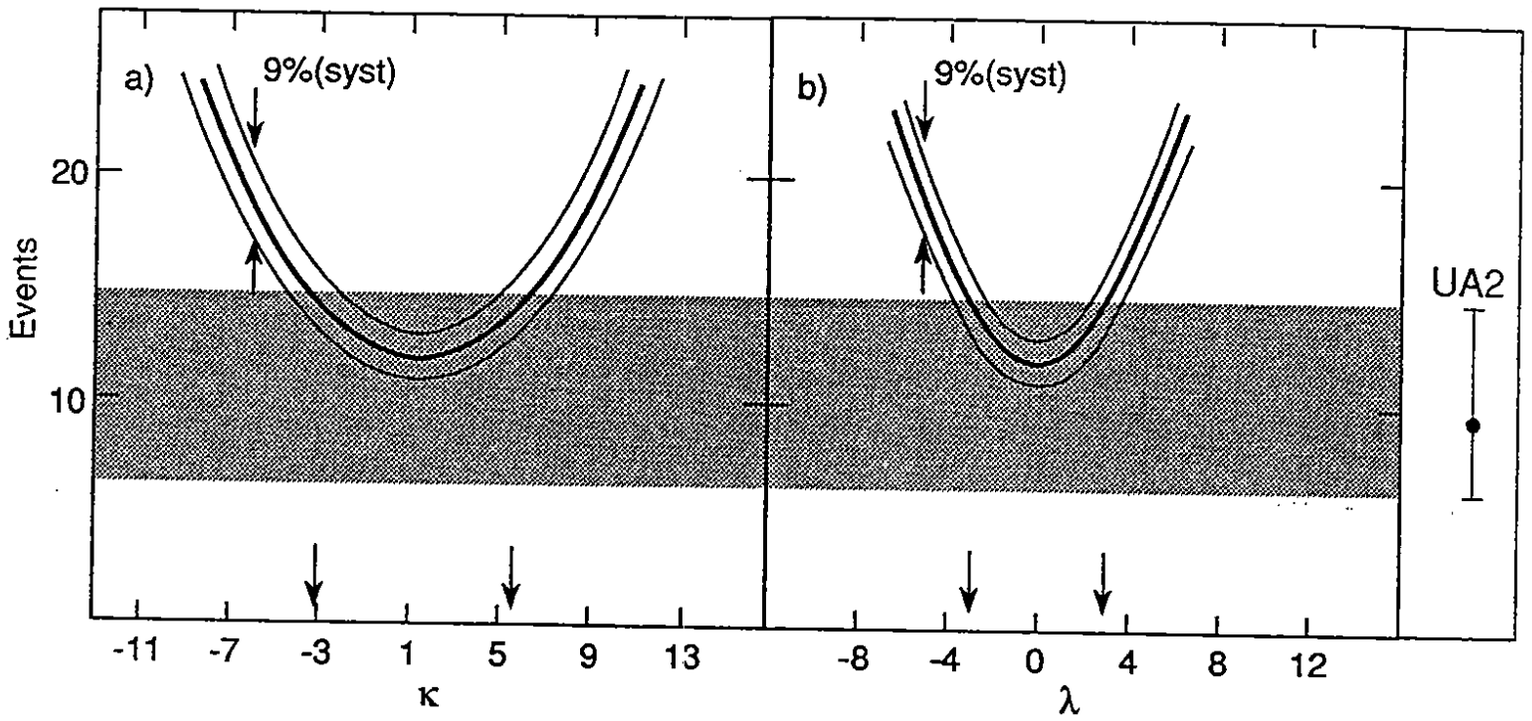
a)
9%(syst)
b)
9%(syst)
UA2
Events
20
10
-11
-7
-3
1
5
9
13
κ
-8
-4
0
4
8
12
λ

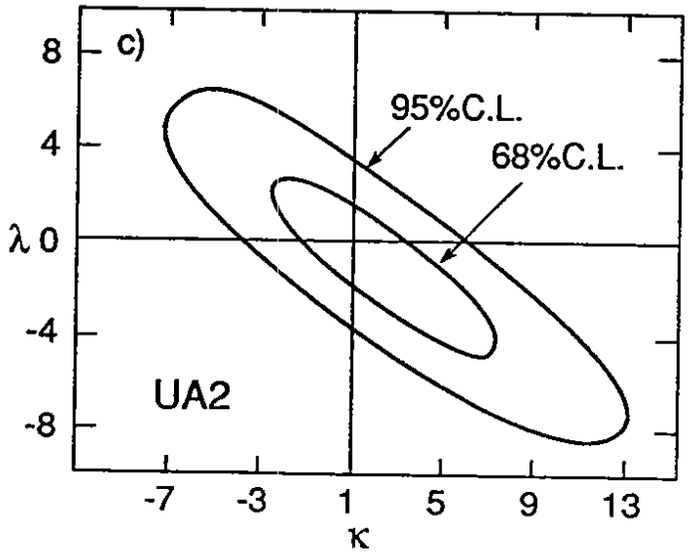
c)
95%C.L.
68%C.L.
UA2
8
4
λ 0
-4
-8
-7
-3
1
5
9
13
κ

FIG. 5

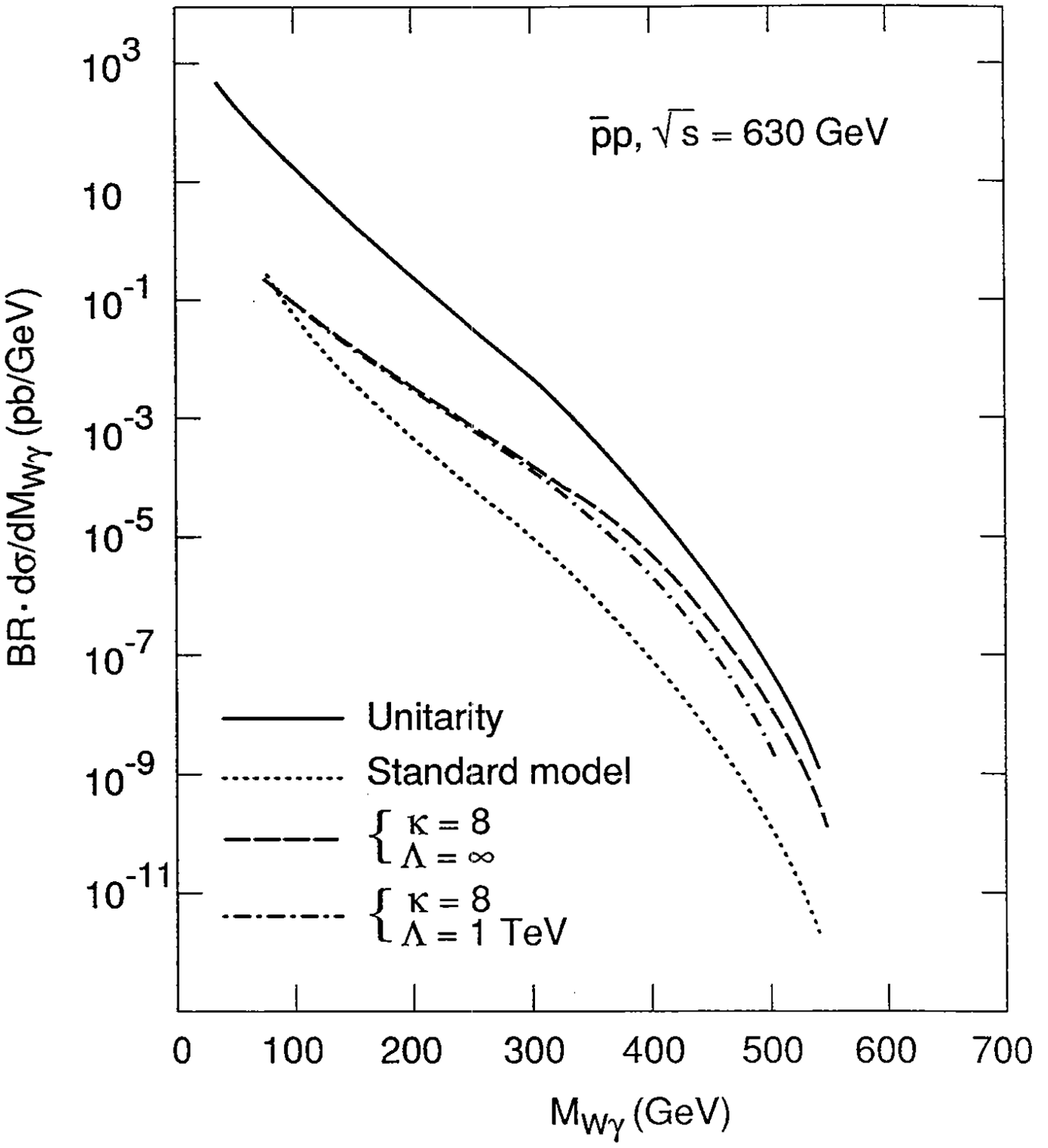

FIG. 6

Imprimé au CERN. Prix : 0.65 Fr.